TOXICOLOGICAL SCIENCES **64,** 122–134 (2001)

Dosimetry Modeling of Inhaled Formaldehyde: The Human Respiratory Tract

John H. Overton,*,[1] Julia S. Kimbell,† and Frederick J. Miller†

*Experimental Toxicology Division, National Health and Environmental Effects Research Laboratory, Office of Research and Development, U.S. Environmental Protection Agency, Research Triangle Park, North Carolina 27711; and †CIIT Centers for Health Research, P.O. Box 12137, 6 Davis Drive, Research Triangle Park, North Carolina 27709

Received March 26, 2001; accepted August 4, 2001

Formaldehyde (HCHO), which has been shown to be a nasal carcinogen in rats and mice, is used widely and extensively in various manufacturing processes. Studies in rhesus monkeys suggest that the lower respiratory tract may be at risk and some epidemiologic studies have reported an increase in lung cancer associated with HCHO; other studies have not. Thus, an assessment of possible human risk to HCHO exposure based on dosimetry information throughout the respiratory tract (RT) is desirable. To obtain dosimetry estimates for a risk assessment, two types of models were used. The first model (which is the subject of another investigation) used computational fluid dynamics (CFD) to estimate local fluxes in a 3-dimensional model of the nasal region. The subject of the present investigation (the second model) applied a 1-dimensional equation of mass transport to each generation of an adult human symmetric, bifurcating Weibel-type RT anatomical model, augmented by an upper respiratory tract. The two types of modeling approaches were made consistent by requiring that the 1-dimensional version of the nasal passages have the same inspiratory air-flow rate and uptake during inspiration as the CFD simulations for 4 daily human activity levels. Results obtained include the following: (1) More than 95% of the inhaled HCHO is predicted to be retained by the RT. (2) The CFD predictions for inspiration, modified to account for the difference in inspiration and complete breath times, are a good approximation to uptake in the nasal airways during a single breath. (3) In the lower respiratory tract, flux is predicted to increase for several generations and then decrease rapidly. (4) Compared to first pulmonary region generation fluxes, the first few tracheobronchial generations fluxes are over 1000 times larger. Further, there is essentially no flux in the alveolar sacs. (5) Predicted fluxes based on the 1-dimensional model are presented that can be used in a biologically based dose-response model for human carcinogenesis. Use of these fluxes will reduce uncertainty in a risk assessment for formaldehyde carcinogenicity.

Key Words: **formaldehyde; upper respiratory tract; respiratory tract; dosimetry modeling; computational fluid dynamics; mass transport; nasal airway.**

Formaldehyde is widely used in various manufacturing processes including the production of wood products, textiles, rubber, and cement and is also commonly used as an intermediate in the synthesis of other industrial chemicals. Worldwide production of formaldehyde is in the millions of tons each year. Swenberg and colleagues (1980) published interim bioassay results on the nature of the squamous cell carcinomas (SCC) caused by formaldehyde inhalation that was expanded upon by Kerns *et al.* (1983), showing formaldehyde to be a nasal carcinogen in rats and mice. These bioassay results had pronounced ramifications on the use of formaldehyde. For example, the U.S. Consumer Product Safety Commission (1982) banned the use of urea-formaldehyde foam insulation.

Since the lowest level (6 ppm) of formaldehyde that induced SCC in rats was less than an order of magnitude greater than some past occupational exposures, there was significant concern about potential carcinogenic risk to humans. Since the early 1980s, various groups have made qualitative or quantitative assessments of formaldehyde carcinogenicity in humans. For example, the International Agency for Research on Cancer (IARC) first published an assessment of formaldehyde in 1982 and subsequently updated their assessment in 1987 and in 1995 (IARC, 1982, 1987, 1995). IARC classifies formaldehyde as probably carcinogenic to humans.

Other groups, such as the U.S. Environmental Protection Agency (U.S. EPA) and Health and Welfare Canada (1987) have developed quantitative risk assessments for formaldehyde. Knowledge of the nature of the exposure-dose-response relationship is integral to quantitative risk assessments. Representations of this relationship have evolved over time as additional knowledge has been brought to bear. In the first quantitative assessment of cancer risk by the U.S. EPA (1987), dose

This manuscript has been reviewed in accordance with the policy of the National Health and Environmental Effects Research Laboratory, U.S. Environmental Protection Agency, and approved for publication. Approval does not signify that the contents necessarily reflect the views and policies of the Agency, nor does mention of trade names or commercial products constitute endorsement or recommendation for use.

[1] To whom correspondence should be addressed at MD-82, National Health and Environmental Effects Research Laboratory, U.S. Environmental Protection Agency, Research Triangle Park, NC 27711. Fax: (919) 541-0026. E-mail: overton.john@epamail.epa.gov.

was represented by the atmospheric concentration of formaldehyde. The incidence of nasal SCC in rats from the Kerns *et al.* (1983) study was the response of interest. The dose-response curve was represented by the linearized multistage model (LMS), an empirical model that does not incorporate any mechanistic data. Significant uncertainty in risk assessment estimates obtained in this earlier approach arose both from the lack of data on interspecies differences in dose and the lack of knowledge of a mechanistic basis for the dose-response curve.

In the early 1990s, the U.S. EPA (1991) developed a risk assessment for the carcinogenicity of formaldehyde that used DNA–protein cross-links (DPX) formed by formaldehyde as an indirect measure of dose. DPX data were available in rats and monkeys. Using DPX data helped decrease uncertainties arising from species extrapolation given that the monkey nose is more similar in structure to the human nose than is the rat nose. The unit risks developed by EPA based on rat and monkey DPX data were 6-fold and 50-fold lower, respectively, than the unit risk calculated in the agency's 1987 assessment.

Concerns about the use of DPX based upon acute exposures of rodents to formaldehyde to represent dose when chronic exposures of people are of interest led to additional research on DPX formation with repeated exposures to formaldehyde. In 1994, Casanova and coworkers showed that rats exposed to a single 3-h exposure of 0.7 or 2 ppm formaldehyde had levels of DPX similar to those in rats exposed subchronically (6 h/day, 5 days/week for 59 exposures). At higher exposure levels, the yield of DPX in chronically exposed animals was about half that of naive rats. These results supported the use of DPX data from acute or chronic formaldehyde exposure studies in the development of risk estimates within the range of current human exposures.

In the meantime, the U.S. EPA (1991) updated their risk assessment using DPX data for both rats and monkeys but continued to use the LMS model. Risk estimates in the 1991 EPA assessment were about 6-fold and 50-fold lower than those obtained in 1987 depending on whether the rat or monkey DPX data were used, respectively. EPA used DPX as an internal dosimeter to help decrease the uncertainty associated with interspecies extrapolation. Despite the highly nonlinear relationship between DPX and tumor incidence, concern about the possible mutagenic potential of formaldehyde at low exposure levels was a major factor in the EPA's continued use of the LMS model.

DPX observed at proximal portions of the rhesus monkey lower respiratory tract (Casanova *et al.,* 1991) suggested that, in addition to the upper respiratory tract, the lower respiratory tract may be at risk. In addition, some epidemiologic studies (Blair *et al.,* 1986, 1990; Gardner *et al.,* 1993) reported an increase in lung cancer associated with formaldehyde exposure while others reported no such increases (Collins *et al.,* 1997; Stayner *et al.,* 1988). Thus, an assessment of potential risk from formaldehyde exposure based on dosimetry information throughout the respiratory tract is appropriate.

Formaldehyde dosimetry models needed to be developed for humans to underpin a biologically based, 2-stage clonal growth model for formaldehyde carcinogenicity. Researchers at the Chemical Industry Institute of Toxicology (CIIT) Centers for Health Research have developed a 3-dimensional, anatomically accurate CFD model for nasal airflow in the human (Subramaniam *et al.,* 1998). This model has been used to estimate the dose or flux (rate of transport) of formaldehyde into tissue at specific locations in the nasal region (Kimbell *et al.,* 2001a,b). In the present work, we describe a 1-dimensional dosimetry model developed for the uptake of formaldehyde in the respiratory tract of humans and present predicted fluxes that can be used (along with the nasal fluxes of Kimbell *et al.,* 2001b) in a formaldehyde risk assessment.

The dosimetry model presented estimates the flux of formaldehyde to tissue in each airway passage, airway, and airspace of the respiratory tract by the use of 1-dimensional mass transport equations applied to a Weibel-type anatomical model of the lower respiratory tract, augmented by an upper respiratory tract. This 1-dimensional dosimetry model was calibrated so that results for the 1-dimensional nasal airway agreed with the CFD model predictions of Kimbell *et al.* (2001b) for a 3-dimensional nasal airway model during inspiration. Since humans switch to oronasal breathing when ventilatory demand exceeds about 35 l/min (Niinimaa *et al.,* 1980, 1981), a portion of the inhaled air is not filtered by the nose, thereby reducing nasal airway flux, but increasing penetration of formaldehyde to the lower respiratory tract. Thus, the 1-dimensional dosimetry model was developed in such a way that oronasal breathing can be taken into account. This capability is critical because a risk assessment for humans needs to account for the various breathing patterns that are associated with human activity levels. For the present work, flux to tissue is determined for 4 daily activity levels.

For a risk assessment, regional flux predictions would consist of the nasal fluxes described by Kimbell *et al.* (2001b) and the 1-dimensional predictions for the rest of the respiratory tract (RT), presented here. This allows for another iteration of quantitative risk estimation that maximally incorporates toxicological, mechanistic, and dosimetric data on formaldehyde to develop a biologically based dose-response model. Further, cancer risk estimates, based on these regional flux predictions, will incorporate significantly less uncertainty in interspecies extrapolation of response than previous risk assessments.

METHODS

In this section the 1-dimensional path anatomical model is described. This model is referred to as an "identical-path" anatomical model, because all paths from the nose or mouth entrance to alveolar sacs are identical. The 1-dimensional mass transport dosimetry model and associated parameters are discussed. Also described are the methods of modeling uptake during oronasal breathing and the procedure used so that the uptake results of the 1-dimen-

TABLE 1
Activity States and Ventilatory Parameters for an Adult Male

Activity state	Breathing mode	Volume (l/min)			Breaths/min
		Minute	Inspired nasal region airflow	Tidal volume	
Sleeping	Nasal	7.5	15	0.625	12
Sitting	Nasal	9	18	0.750	12
Light exercise	Nasal	25	50	1.250	20
Heavy exercise	Oronasal	50	46[a]	1.923	26

Note. Activity states and ventilatory parameters for an adult male as defined in ICRP66 (1994).
[a]For the oronasal breathing state, only 46% of the inhaled air flows through the nasal region.

sional model nasal region is consistent with the CFD predictions of Kimbell *et al.* (2001b). (In this report, the term "nasal" refers to that region of the upper respiratory tract from the nostrils through the nasopharynx.)

Definition of hypothetical human and activity states. The exposed human was defined as an adult Caucasian male having a height, age, and weight of 176 cm, 30 years, and 73 kg, respectively (ICRP66, 1994). This definition determined the choice of other characteristics such as ventilation and respiratory tract anatomical dimensions. Depending on a person's occupation or daily routine, time will be spent at different levels of exertion; further, depending on the occupation, the time spent at similar levels of exertion generally will be different. Different activities or levels of exertion can result in substantially different doses of inhaled formaldehyde to respiratory tract tissues. In order to account for variations in dose due to occupation and/or daily routine, simulations were carried out for 4 exertion levels or activity states given by ICRP66 (1994) for the hypothetical adult male. The activities are given in Table 1, along with minute volume, inspired nasal airflow rate, tidal volumes, breathing frequency, and other information, all of which were needed to perform a simulation for each activity state.

For consistency with Kimbell *et al.* (2001b), we assumed constant inhalation and exhalation flow rates and equal inhalation and exhalation times. Thus, for nasal breathing the flow rates for the CFD steady-state simulations are twice the minute volume. (Table 1). At a minute volume of 50 l/min, oronasal breathing occurs for most people with 46% of the air passing through the nasal passages (ICRP66, 1994), so that the steady-state inspiratory flow rate in the human nasal passage is 46 l/min.

Computational fluid dynamics nasal passage model. CFD modeling of the nasal passages is described in detail elsewhere (Kimbell *et al.*, 2001a,b; Subramaniam *et al.*, 1998). A brief summary is given here. Local nasal flux of formaldehyde (HCHO) from inhaled air to the air-lining interface was estimated from CFD steady-state simulations of unidirectional inspiratory airflow and HCHO transport equations conducted using a 3-dimensional, anatomically accurate reconstruction of the nasal passages of an adult human male.

The transport of inhaled formaldehyde in the nasal passages was assumed to occur by inspiratory airflow, molecular diffusion, and airway surface absorption. Airflow velocities were estimated from simulations of steady-state inspiratory airflow using the human nasal CFD model. The airflow simulations required the numerical solution of the Navier-Stokes equations of motion for incompressible Newtonian fluid flow.

Airflow and uptake simulations were conducted for nasal inspiratory rates of 15 and 18 l/min, but simulations at 46 and 50 l/min were beyond available computer resources (Kimbell *et al.*, 2001b). Thus, additional CFD simulations were performed at intermediate inspiratory rates and the uptake results were extrapolated to the higher flow rates. Kimbell *et al.* (2001b) reported predicted nasal HCHO uptake values as 75.9, 71.8, 56.4, and 55.2% at nasal inspiratory rates of 15.0, 18.0, 46, and 50 l/min, respectively (corresponding to minute volumes of 7.5, 9.0, 50, and 25 l/min).

Identical-Path Respiratory Tract Dosimetry Model

Anatomical model. Ideally, an anatomical model of the respiratory tract should simulate all of the paths (each being unique) from the upper respiratory tract (URT) entrance to the most distal airspaces. Unfortunately, use of such a model for gases is beyond our present calculational resources. Therefore, anatomical characteristics of the respiratory tract are represented by a single-path, symmetric, or an identical-path anatomical model. For the purpose of this investigation, these types of models are equivalent to the assumption that all paths are identical. Thus, for a given generation or model segment, the dimensions of one airway or airspace and the number of airways or airspaces in the generation completely define the characteristics of the given anatomical model generation. As a consequence, only one path needs to be considered, making the respiratory tract dosimetry modeling of HCHO feasible. The use of identical-path type anatomical models is well established for respiratory tract dosimetry modeling (e.g., Miller *et al.*, 1985; Overton *et al.*, 1996; Paiva, 1973; Scherer *et al.*, 1972, 1988).

URT model segments are identified by negative integers (Table 2) that increase distally from the nose or mouth entrance to the last URT segment (–1) that is just proximal to the trachea, defined as generation 0. Beginning with the trachea and proceeding distally, lower respiratory tract generations are identified by increasing integers. Thus, model segments from the beginning of the respiratory tract to the alveolar sacs are identified by a continuous sequence of increasing integers. Although only the lower respiratory tract (LRT) model segments correspond to generations, URT segments will often be referred to as "generations" for convenience.

There are 2 anatomical models for the URT, one for oral airflow and one for nasal airflow. Table 2 gives the dimensions of the segments. Both URT models are composed of 2 main segments (–2 and –1) and a "numerical segment" (–3). This latter segment was added for numerical purposes: to force the boundary conditions to be equivalent to that of the CFD simulations. This segment does not correspond to any real anatomical region or location and does not absorb HCHO. Its inclusion in Table 2 is for completeness and the reason for its use is discussed at greater length in the Appendix.

The main URT segments correspond to the "proximal" and "distal" URT. The proximal URT (segment –2) represents either the mouth cavity or the (identical-path) nasal airway passage, but not both. The distal URT (segment –1) is defined as the air passage distal to both the nasal airway and the mouth cavity; it begins at the proximal oropharynx and ends at the proximal end of the trachea. For the mouth cavity and the distal URT, the choice of a constant diameter geometry is consistent with Fredberg *et al.* (1980). The rationale for also using this simple geometry for the nasal airways relates to use of the CFD predictions, and not the identical-path model predictions, to define local fluxes within the nasal airways; thus, the identical-path model only needs to remove HCHO from the inhaled air at the same rates as predicted by the 3-dimensional CFD model simulations; for this, a detailed structure is not necessary.

The geometry and dimensions of the LRT (Table 3) are based on the identical-path anatomical model of Weibel (1963), with the dimensions iso-

TABLE 2
Structural and Dimensional Characteristics of the Identical-Path Upper Respiratory Tract Anatomical Models

Region	Model segment no.	Diameter	Length	Volume	Surface area
URT model for airflow through nasal airway					
Numerical segment[a]	–3	0.537	0.5	1.1	8.2
Nasal airway[b]	–2	0.537	15.0	33.0	246.0
Distal URT[c]	–1	1.784	15.0	37.5	84.1
Total			30.5	71.6	338.3
URT model for airflow through mouth cavity					
Numerical segment[d]	–3	1.784	0.5	1.25	2.80
Mouth cavity[c]	–2	1.784	10.0	25.0	56.1
Distal URT[c]	–1	1.784	15.0	37.5	84.1
Total			25.5	63.75	143.0

Note. Measurements of length are given in cm, volume in cm, area in cm^2.

[a]Defined as having the same diameter as the nasal airway and an arbitrary but short length of 0.5 cm, which is one-thirtieth the length of the nasal airway; volume is defined as one-thirtieth those of the nasal airway volume. Actual value of surface area is irrelevant since the mass transfer coefficient of the segment is 0.

[b]Surface area and volume values are those of the 3-dimensional reconstructed human nasal airway; length estimated from Subramaniam *et al.* (1998); diameter is the hydraulic diameter: 4 × volume/(surface area).

[c]Distal URT and mouth cavity dimensions are based on Fredberg *et al.* (1980) who gave plots of cross sectional areas versus distance. The dimensions reflect our assumption of a tube geometry with constant, circular cross sectional area.

[d]Defined as having the same diameter as the mouth cavity and an arbitrary but short length of 0.5 cm, which is one-twentieth the length of the mouth cavity; volume is defined as one-twentieth of the cavity volume. Actual value of surface area is irrelevant since the mass transfer coefficient of the segment is 0.

tropically scaled to correspond to regional volumes based on ICRP66 (1994), Hart *et al.* (1963), and Fredberg *et al.* (1980). The Weibel model is equivalent to a symmetric branching structure such that each airway or duct bifurcates into identical daughters, with each generation having twice as many airways or ducts and alveoli as the previous generation.

Because the dosimetry model takes into account expansion and contraction, LRT dimensions change during the breathing cycle. The trachea is assumed to be rigid. Proceeding distally from the trachea, the TB airways are assumed to increase in compliance such that the fractional change in the volume of an airway above its functional residual capacity (FRC) value increases jointly with the inhaled volume and the generation number (the increase in generation number simulates the increase in compliance). This relationship holds up to and including the first pulmonary region generation. The pulmonary region expands and contracts uniformly: the fractional change in the airspace volume of each pulmonary region generation changes in the same proportion to inhaled volume as the fractional change in volume does in the first pulmonary region generation. Dimensions are assumed to change isotropically.

Mass transport model. In each model segment, HCHO transport and uptake are approximated by a 1-dimensional convection-dispersion equation that accounts for inhalation and exhalation, expansion and contraction, convection, dispersion, molecular diffusion, and absorption at the air-liquid lining surface. Inhalation and exhalation times are assumed equal; airflow rates are constant and equal to twice the minute volume during both inhalation and exhalation; i.e., the airflow rate is in the form of a square wave. The rationale for this latter assumption is to maintain consistency with the CFD simulations, which used constant airflow rates. A mathematical description of the model is given in the Appendix.

In order to account for oronasal breathing in the identical-path model, two simulations were used. In 1 simulation, the nasal airway model was used for the proximal URT; in the other, the mouth cavity model was used for this region (see Table 2). In these simulations, the airflow rate that would occur in the mouth cavity or in the nasal airways during oronasal breathing was taken into account. The airflow rate in all segments distal to the proximal URT corresponded to that expected for the full minute volume of 50 l/min. The same airflow rate split was assumed for both inhalation and exhalation. For each corresponding segment distal to the proximal URT, the fluxes of HCHO from both simulations were added to obtain the estimated dose for oronasal breathing.

The rationale for the approach to oronasal breathing dosimetry is presented in the Appendix. Also in the Appendix, issues concerning the accuracy of the numerical procedure used to solve the equation of mass transport, solution convergence, and mass conservation are discussed.

Calibration of identical-path nasal passage uptake to CFD nasal passage uptake. For the identical-path simulation results to be meaningful, the percent uptake predictions for the identical-path nasal airway were required to agree with the CFD predictions. To obtain this, overall mass transfer coefficients were estimated for the identical-path nasal airway (segment –2, Table 2), so that percent uptakes were in agreement with the CFD results.

The identical-path dosimetry model was used to simulate the CFD results, but the model had the following modifications: (1) Except for the nasal airway model, uptake in all other model segments was required to be 0. (2) Parameters were set to obtain the correct inhaled airflow rates and to obtain steady state by the end of the inhalation phase (which was made long as necessary to obtain steady state). Simulations were carried out for different values of the identical-path nasal airways overall mass transport coefficients until a value was found for which the percent uptake at steady state matched the appropriate CFD simulation value to within 0.2%. The resulting overall identical-path nasal airway mass transfer coefficients, corresponding to minute volumes of 7.5, 9.0, 25, and 50 l/min (nasal steady-state inspired rates of 15, 18, 50, and 46 l/min), were 1.68, 1.78, 2.98, and 2.83 cm/s, respectively.

As a check on the agreement between the 1-dimensional dosimetry calibration and CFD simulation results, the predicted average nasal airway surface fluxes were compared. Table 4 presents the CFD model and calibration results for comparison in columns 3 and 4, respectively; these results indicate that the CFD predictions and identical-path average nasal passage surface fluxes differ by less than 0.7% (remaining table entries are discussed later).

RESULTS

In order to understand how the CFD predictions of inspiratory HCHO nasal uptake can be applied to cyclic breathing

TABLE 3
Structural and Dimensional Characteristics of the Modified Weibel (1963) Single-Path Lower Respiratory Tract Anatomical Model at Functional Residual Capacity

Comments	Z[a]	No. of airways	Airway or duct dimensions			Alveolar volume (ml)	Surface area (cm^2)[b]
			Diameter (cm)	Length (cm)	Volume (ml)		
Tracheobronchial region							
Trachea	0	1	1.467	9.788	16.55	—	45.12
	1	2	1.000	3.882	6.10	—	24.40
	2	4	0.665	1.549	2.15	—	12.95
	3	8	0.460	0.619	0.82	—	7.17
	4	16	0.379	1.035	1.87	—	19.76
	5	32	0.285	0.872	1.78	—	25.06
	6	64	0.227	0.733	1.91	—	33.61
	7	128	0.183	0.619	2.08	—	45.61
	8	256	0.151	0.521	2.41	—	63.64
	9	512	0.125	0.440	2.80	—	89.09
	10	1024	0.105	0.375	3.36	—	127.44
	11	2048	0.089	0.318	4.09	—	183.14
	12	4096	0.078	0.269	5.32	—	271.47
	13	8192	0.069	0.220	6.74	—	391.02
	14	16384	0.060	0.187	8.88	—	585.72
	15	32768	0.052	0.163	11.75	—	888.51
Terminal bronchioles	16	65536	0.048	0.134	16.08	—	1334.99
TB region totals				21.731	94.78	—	4148.78
Pulmonary region							
1st Respiratory bronchioles	17	131,072	0.047	0.123	28.36	4.27	3366.25
2nd Respiratory bronchioles	18	262,144	0.044	0.102	41.46	14.25	6960.31
3rd Respiratory bronchioles	19	524,288	0.042	0.087	63.24	42.75	15,469.77
	20	1,048,576	0.039	0.072	94.67	149.64	44,018.44
	21	2,097,152	0.038	0.061	152.21	295.68	87,264.63
	22	4,194,304	0.037	0.051	237.52	598.56	175,301.51
Alveolar sacs	23	8,388,608	0.037	0.043	401.07	1018.97	298,089.78
Pulmonary region totals				0.544	1018.57	2124.14	630,470.75
LRT totals				22.274	1113.35	2124.14	634,619.53

Note. Based on the ICRP66 (1994) reference values for males with age, height, weight, and functional residual capacity (FRC) of 30 years, 176 cm, 73 kg, and 3300 ml, respectively. Anatomical dead space (V_D = oral passage volume + TB region volume) is based on an equation for anatomical dead space of Hart *et al.* (1963) for males: $V_D = (3.846E\text{-}4)\text{height}^{2.499} = 157.2$ ml. The volume of the oral passage (V_O) is 62.5 ml (inferred from Fredberg *et al.*, 1980). Thus, LRT volume = FRC – V_O = 3237.5 ml and the TB region volume = $V_D - V_O$ = 94.7 ml.

[a]Generation.

[b]In pulmonary region, includes alveolar surface area.

conditions, the identical-path dosimetry model predictions of total nasal airway uptake during inhalation and for a complete breath are discussed. Table 4 presents predicted average surface flux for the nasal airways during the inhalation phase of the first breath (column 5) and for the first complete breath (column 6). The averaging time for both fluxes is based on the same time span of one breath. For each of the 4 breathing states, the difference between the two fluxes is less than 3%. Note that the entries in columns 5 and 6 are also the values predicted for "steady state;" that is, nasal airway fluxes are predicted to be the same for each breath regardless of how many breaths have been taken. The significance of this is that, at all times, all but 3% of the nasal airway uptake occurs during inhalation so that HCHO exhaled from the lower respiratory tract does is predicted not to significantly affect the flux to nasal tissues during a complete breath. Consequently, for the CFD nasal airways, the breath average flux can be defined as one-half the CFD dosimetry estimate.

For the identical-path model, calibration results and nasal uptake during the inhalation phase of a complete breath are presented in Table 4 for comparison. The calibration surface fluxes (column 4) are approximately twice the fluxes during inhalation for which the averaging time is the breath time (Table 4, column 5). However, since the mass was absorbed during inhalation, which is assumed to be one-half the breath time, the average surface flux based on the inhalation time is twice that in column 5. Based on this time averaging, the calibration results (column 4) and the surface flux during inhalation (twice the values in column 5) differ by less than 3% for nasal breathing and about 7% for oronasal breathing. That

TABLE 4
Comparison of Average Nasal Airway Fluxes Predicted during Different Simulation Conditions

		Average surface flux for the nasal airway (pmoles/h-ppm-mm^2)			
			Single path dosimetry model		
Minute volume (l/min)	Unidirectional airflow rate[a] (l/min)	CFD[b] results	Calibration to CFD results	FIB[c]	FIEB[d]
Column 1	Column 2	Column 3	Column 4	Column 5	Column 6
7.5[e]	15	1,136	1,134	552	568
9.0[e]	18	1,290	1,292	630	648
25.0[e]	50	2,752	2,756	1,354	1,391
50.0[f]	46	2,587	2,584	1,213	1,247

[a] The unidirectional or the inhalation flow rate in the nasal airway is twice the minute volume for nasal breathing; for oronasal breathing, the nasal airway unidirectional or inhalation airflow rate is 0.46 times twice the minute volume.
[b] Kimbell *et al.* (2001b).
[c] FIB = the average flux during inhalation based on the time of one breath (that breath being the first breath as well as any other breath). Let T = the time length of one breath and MI = the mass absorbed per unit area during inhalation. Then FIB = MI/T.
[d] FIEB = the average flux for a complete breath based on the time of one breath (that breath being the first breath as well as any other breath). Let ME = the mass absorbed during exhalation. Then, FIEB = (MI + ME)/T.
[e] Nasal breathing.
[f] Oronasal breathing.

they differ is expected because the calibration simulations and the simulations that resulted in column 5 were carried out with different conditions (i.e., no absorption distal to the nasal airways occurred for the calibration simulations, whereas for the other identical-path simulations, the distal airways did absorb).

For each model generation, Table 5 lists the average surface fluxes predicted by the identical-path dosimetry model as well as the results of the two simulations that were combined to estimate the oronasal breathing fluxes. In this table and in Figure 1 the URT segments designated in Table 2 as numerical segments (–3) have been omitted (their purpose is calculational and they do not absorb HCHO). In Table 5, column 1 (columns are indicated in top row of table) specifies the model generation number. Columns 2, 3, 4, and 5 are the fluxes predicted for the 4 ventilation states. Column 5 is also the sum of the values in columns 7 and 9, as indicated by the equal and plus signs in columns 6 and 8, respectively. Columns 7 and 9 are the fluxes of the nasal and oral path simulations that were combined to estimate the oronasal fluxes given in column 5. "N/a" is placed in column 5, generation –2, because there are 2 proximal URT fluxes for oronasal breathing, the nasal airway and the mouth cavity fluxes; these fluxes are listed for generation –2 in columns 7 and 9, respectively.

Figure 1 is a plot of the predicted identical-path fluxes (Table 5) versus generation for the 4 activity states (identified by minute volume), defined in Table 1. The 3 lowest minute volumes correspond to nasal breathing and the largest value to oronasal breathing. For the latter, the proximal 1-dimensional URT (generation –2) flux values are plotted for both the mouth cavity and nasal airway.

From Figure 1 and Table 4 we observe the following: Except for oronasal breathing, the highest surface fluxes are predicted for the nasal airways and mouth cavity. As minute volume increases, HCHO penetrates further into the respiratory tract. For nasal breathing, the average nasal airway flux is at least 2.5 to 3 times greater than predicted for any other model segment or generation. During oronasal breathing (50 l/min minute volume), 46% of the inhaled air flows through the nasal airways (ICRP66, 1994), which corresponds to a rate that is less than for the 25 l/min nasal breathing state. This results in nasal flux during oronasal breathing being less than that for the 25 l/min minute volume nasal breathing state. The peak fluxes that occur at generation 3 are due to 2 competing factors. From generation –1 distally, the overall mass transfer coefficient increases, which tends to increase flux distally. On the other hand, absorption by proximal generations reduces the mass available for absorption. Hence, at some point, the fluxes must decrease, which occurs in generation 3 in the current simulations. The distal decrease in flux is such that the fluxes to pulmonary region surfaces are predicted to be several orders of magnitude smaller than the maximum lower respiratory tract fluxes.

DISCUSSION

Uncertainty in risk estimates based on use of models such as are presented here arises primarily from the assumptions made about model structures and from the choices used for parameter values. In many cases, the justification for the assumption or parameter value lowers its contribution to uncertainty. The development and use of the identical-path models for respira-

TABLE 5
Predicted Respiratory Tract Breath-Averaged Surface Fluxes of Formaldehyde

Column	1 (Z)[a]	2	3	4	5	6	7	8	9
Minute volume (L/min)		7.5	9	25	50		50		50
Breathing mode or path		Nasal	Nasal	Nasal	Oronasal		Nasal path		Oral path
Flux (picomoles/ppm-h-mm^2)									
Proximal URT	–2	5.678E+02	6.476E+02	1.390E+03	n/a[b]		1.247E+03		1.070E+03
Distal URT	–1	1.517E+02	1.956E+02	5.475E+02	1.132E+03	=	3.394E+02	+	7.933E+02
Trachea	0	1.442E+02	1.896E+02	5.434E+02	1.168E+03	=	3.498E+02	+	8.184E+02
	1	1.364E+02	1.823E+02	5.460E+02	1.190E+03	=	3.566E+02	+	8.341E+02
	2	1.421E+02	1.913E+02	5.780E+02	1.256E+03	=	3.762E+02	+	8.801E+02
	3	1.472E+02	1.989E+02	6.023E+02	1.304E+03	=	3.907E+02	+	9.139E+02
	4	1.270E+02	1.740E+02	5.547E+02	1.231E+03	=	3.689E+02	+	8.629E+02
	5	1.095E+02	1.536E+02	5.281E+02	1.201E+03	=	3.599E+02	+	8.419E+02
	6	8.482E+01	1.232E+02	4.769E+02	1.129E+03	=	3.382E+02	+	7.911E+02
	7	5.903E+01	9.018E+01	4.155E+02	1.040E+03	=	3.117E+02	+	7.289E+02
	8	3.496E+01	5.728E+01	3.394E+02	9.228E+02	=	2.764E+02	+	6.464E+02
	9	1.694E+01	3.049E+01	2.568E+02	7.859E+02	=	2.354E+02	+	5.505E+02
	10	6.225E+00	1.268E+01	1.726E+02	6.259E+02	=	1.874E+02	+	4.384E+02
	11	1.602E+00	3.823E+00	9.838E+01	4.521E+02	=	1.353E+02	+	3.167E+02
	12	2.601E-01	7.555E-01	4.423E+01	2.811E+02	=	8.417E+01	+	1.970E+02
	13	2.495E-02	9.160E-02	1.489E+01	1.449E+02	=	4.336E+01	+	1.015E+02
	14	1.326E-03	6.324E-03	3.445E+00	5.765E+01	=	1.724E+01	+	4.040E+01
	15	3.630E-05	2.284E-04	4.935E-01	1.616E+01	=	4.829E+00	+	1.133E+01
Terminal bronchioles	16	5.214E-07	4.291E-06	4.015E-02	2.894E+00	=	8.639E-01	+	2.030E+00
1st Respiratory bronchioles	17	3.483E-09	3.533E-08	1.256E-03	2.157E-01	=	6.427E-02	+	1.514E-01
	18	7.113E-12	8.372E-11	9.643E-06	4.374E-03	=	1.299E-03	+	3.074E-03
	19	8.666E-15	1.098E-13	2.589E-08	2.531E-05	=	7.499E-06	+	1.781E-05
	20	5.864E-18	7.645E-17	2.523E-11	3.850E-08	=	1.136E-08	+	2.713E-08
	21	1.936E-21	2.536E-20	9.397E-15	1.720E-11	=	5.061E-12	+	1.214E-11
	22	1.016E-24	1.325E-23	5.016E-18	9.619E-15	=	2.821E-15	+	6.798E-15
Alveolar sacs	23	8.765E-28	1.135E-26	4.236E-21	8.069E-18	=	2.359E-18	+	5.709E-18

[a]Generation.
[b]Flux for nasal region and mouth is given in columns 7 and 9 respectively.

tory tract formaldehyde uptake required a number of assumptions regarding simulation, parameter specification, and anatomical issues. A discussion of the sources of uncertainty associated with the major assumptions will be given here.

Cyclic breathing simulations conducted using the identical-path model supported the use of CFD steady-state inspiratory dosimetry simulation results as a basis to estimate nasal uptake of formaldehyde during cyclic breathing. This conclusion is based on the identical-path model predictions that during exhalation nasal airway fluxes increase by less than 3% over fluxes during inspiration. Thus, the assumption that the use of the CFD predictions contributes insignificantly to error in estimating nasal flux for a complete breath is reasonable.

The calibration of the identical-path model to the CFD predictions resulted in identical-path model predictions of nasal airway % uptake that were within 0.2% of the CFD model predictions and in average surface fluxes that were within 0.7% of CFD model predictions. Thus, any contribution to uncertainty from the assumption that these two models were appropriately matched is considered low.

Quantification of anatomical sources of uncertainty involves determining the extent to which normal variation in these model inputs affects flux. Based on Overton *et al.* (1996), we infer that for $\pm$ 2 standard deviations in dead space volume the pulmonary region fluxes could be 60% less to 180% more than the flux predicted for an average dead space volume. These investigators also showed that the sensitivity of the fractional uptake due to change in dead space volume decreases as the TB region mass transfer coefficient increases, but the sensitivity of the pulmonary region uptake increases. Since the HCHO mass transfer coefficients are at least 4 times as large as those used by Overton *et al.* (1996) for ozone, we infer that uncertainty in the dead space volume has a negligible effect on fractional uptake, but can affect the pulmonary region distribution of flux.

Another anatomical issue is the assumption of identical paths. As this assumption does not strictly hold in reality, there would be in each generation a distribution of fluxes due to the different paths and different airways of the human LRT. An estimated upper limit to which flux may vary in a given generation may be inferred from Overton and Graham (1995) who simulated ozone uptake in the asymmetric branching airways of rats. They predicted that the ratio of the highest to

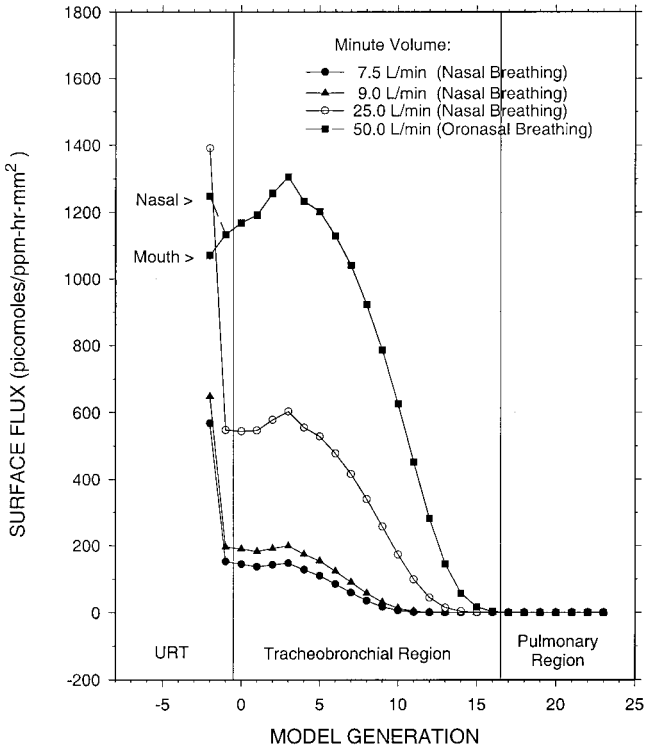

FIG. 1. The identical-path dosimetry predictions of surface flux versus generation for each of the 4 activity modes.

lowest flux in the same TB generation could be as high as 7, the average ratio being 3. Since the human LRT is considered much more symmetric than that of the rat (Phalen and Oldham, 1983), flux variation among airways in a human TB generation should be less than for the rat.

In the dosimetry model, gas phase mass transfer coefficients and dispersion coefficients were based on formulas derived by investigators using conditions often different than those in the present work. For example, the URT gas phase mass transfer coefficients given by Nuckols (1981) are not defined locally, as used as in the present investigation; they are representative coefficients for the regions from the nostrils or lips to the trachea. Further the values of the air speed and diameter (Appendix; Equations 11 and 12) used to calculate the transfer coefficient are defined by Nuckols (1981) to be those of the trachea. We used local values for these parameters, which is reasonable, since the mass transfer coefficient is positively correlated with air speed and diameter. A method for converting formulas and their predictions obtained under one set of conditions to different conditions would be useful.

Respiratory tract air was approximated as being dry with no contaminants other than HCHO. In reality, respiratory tract air contains water, carbon dioxide, and inhaled contaminants that may affect the transport of HCHO. Under normal conditions, gaseous contaminants are generally at low enough partial pressures to have little effect on the mass transfer of HCHO. Conceivably, aerosols could be a source of HCHO. In addition, moving throughout the airways, aerosols have the potential to absorb and desorb HCHO, altering the distribution of HCHO uptake. The absorption or desorption of water vapor at the air-liquid lining interface may enhance or reduce, respectively, the transfer of HCHO to this interface. Although the inclusion of these processes are beyond the scope of this investigation, we consider the assumption of dry air with no contaminants as being a reasonable approximation.

Overall, the use of local respiratory tract dosimetry modeling in calculating human cancer risk estimates should represent a significant reduction in uncertainty over previous risk assessments. The 1987 and 1991 formaldehyde cancer risk assessments (U.S. EPA, 1987, 1991) were based on the linearized multistage model using as measures of dose the inhaled concentration of formaldehyde and DPX, respectively. Major uncertainties in these risk assessments arose from the assumptions that uneven distribution of inhaled formaldehyde over the nasal surface and differences in these distributions between rats and humans were not consequential. Site-specific nasal lesions observed in rats and primates (Monticello *et al.*, 1989, 1991) suggest that there is significant local species-specific variation in formaldehyde. The same can be inferred about the LRT.

In summary, HCHO, which is used widely and extensively in various manufacturing processes, has been shown to be a nasal carcinogen in rats and mice. Further, studies in monkeys suggest that the LRT may be at risk and some epidemiological studies have reported an increase in lung cancer associated with HCHO, whereas other studies have not. Thus, an assessment of possible human risk to HCHO exposure throughout the respiratory tract is desirable, requiring dosimetry information in the RT. To this end, two types of dosimetry models were used to provide predictions of local HCHO surface fluxes (dose). The first type of dosimetry model is based on a 1-dimensional equation of mass transport applied to each generation airway and airway passage of a symmetric, bifurcating RT anatomical model. This model is the subject of the present investigation. For the second type, CFD techniques were used to estimate total uptake and local surface fluxes in a 3-dimensional model of the nasal region (Kimbell *et al.*, 2001a,b). The 1-dimensional model was calibrated so that the predicted uptake in its nasal airways model agreed with the human nasal region uptake results of the CFD simulations of Kimbell *et al.* (2001b). Simulations for both model types were carried out for an adult human male and 4 activity states (4 different sets of ventilatory parameters). The two types of modeling approaches were made consistent by requiring that the 1-dimensional version of the nasal passages have the same uptake during inspiration as the CFD results for each human activity level. Thus, the estimated surface fluxes for the human are defined as the CFD predictions for the nasal region plus the 1-dimensional model predictions of local flux in the rest of the RT.

Results obtained include the following: (1) For each activity state, more than 95% of the inhaled HCHO is predicted to be retained by the RT. (2) The CFD predictions for inspiration,

modified to account for the difference in inspiration and complete breath times, are predicted by the 1-dimensional to be a good approximation to uptake by the nasal airways during a single breath. (3) In the lower respiratory tract, flux is predicted to increase for several generations and then decrease rapidly. (4) Compared to first pulmonary region generation fluxes, the first few tracheobronchial generations fluxes are over 1000 times larger. Further, there essentially is no flux in the alveolar sacs. (5) The predicted fluxes, based on the 1-dimensional model that are presented here, can be used in a biologically based dose-response model for human carcinogenesis and should reduce uncertainty in a risk assessment.

APPENDIX

RATIONALE FOR NUMERICAL SEGMENT IN IDENTICAL-PATH MODEL

Because velocity was modeled as uniform across the nostril entrance, the CFD boundary conditions at this location resulted in a negligible dispersion, and the rate of HCHO influx was equivalent to the product of airflow rate and the exposure concentration. For the identical-path simulations, the boundary condition at the nostril entrance during inhalation was a constant concentration, which does not limit the rate of HCHO influx to the airflow rate times the exposure concentration, as in the CFD case. If the concentration gradient and the dispersion coefficient are sufficiently large, the flux due to dispersion can alter the HCHO influx so as to be significantly different than the product of airflow rate and exposure concentration. To account for this in the identical-path formulation, a short, small nonabsorbent segment (numerical segment, Table 2) was added proximal to the nostrils, resulting in a negligible dispersion as required. (See Equation 9 for the relationship between the dispersion coefficient and the length of a segment.) Similarly, based on the assumption of small dispersion at the mouth entrance, a small nonabsorbent volume was added proximal to this region (see Table 2).

Identical-Path Model of Mass Transport

The identical-path anatomical model is divided into sequential segments in which anatomical dimensions are, in general, a function of time throughout each breath. In this work, model segments correspond to airways or airspaces; also, there is a one-to-one correspondence between a LRT model segment and each airway or airspace in a specific LRT generation. Further, each airway or airspace in the same generation or model segment is assumed to have the same transport characteristics, such as airflow rate, effective dispersion coefficient, and the overall mass transfer coefficient.

Equation of mass transport for one model segment or airway. For an expanding or contracting airway, air passage, or airspace, a coordinate system is defined such that the x-axis is along the direction of the mean air flow and the origin is at the entrance of the airway (for simplicity, the term "airway" is also used for air passage and airspace). The cross-sectional area of the airway, A(t), is perpendicular to the x-axis and is independent of x for the given airway, but is a function of time, t, due to expansion and contraction. The airway length is L(t).

For the mass balance equation, a small compartment in the airway is considered. The left and right boundaries of this compartment, which are perpendicular to the x-axis, are located at $x = z(t)$ and $z + l(t)$, respectively; where

$$z = a \cdot L(t);\ 0 \le a \le 1; \tag{1a}$$

$$l = b \cdot L(t);\ 0 \le b < a;\ 0 \le a + b \le 1. \tag{1b}$$

The mass balance equation for the compartment beginning at z and ending at $z + l$ is approximated by

$$A \cdot J_z \approx A \cdot J_{z+l} + p \cdot l \cdot K_o \cdot C + \frac{\partial}{\partial t}(A \cdot l \cdot C). \tag{2}$$

Definition of terms in Equation 2: $J = J(z,t)$ = average flux of HCHO in the x direction; $p = p(t)$ is the perimeter of the cross-sectional area; $K_o = K_o(t)$ is the overall mass transfer coefficient; $C = C(z,t)$ is the average concentration of HCHO in the compartment. The terms J_z and J_{z+l} represent the mass flow rate of HCHO into or out of the compartment at the left- and right-hand boundaries, respectively. The peripheral surface area of the compartment is $p \times l$ and $A \times l \times C$ is the approximate mass of HCHO in the compartment.

Expanding J_{z+l} in a Taylor series about z in terms of l and using Equation 1b, Equation 2 can be written as

$$\frac{\partial}{\partial t}(b \cdot V \cdot C) + b \cdot V \cdot \frac{\partial}{\partial z} J \approx - b \cdot S \cdot K_o \cdot C - \frac{A}{2}(b \cdot L)^2 \frac{\partial^2}{\partial z^2} J_z + \cdots \tag{3}$$

where $V = \cdot L$ and $S = p \cdot L$ are the airway volume and surface area, respectively. Dividing both sides of Equation 3 by b and letting b go to 0 yields

$$\frac{\partial}{\partial t}(V \cdot C) + V \cdot \frac{\partial}{\partial z} J = -S \cdot K_o \cdot C. \tag{4}$$

The flux, J, is defined as

$$J = u \cdot C - D \cdot \frac{\partial}{\partial z} C, \tag{5}$$

$D = D(t)$ is the dispersion coefficient and $u = u(z,t)$ is the air velocity in the x direction.

Replacing J in Equation 4 with the right-hand side of Equation 5 and rearranging, we obtain the spatially 1-dimensional convection-dispersion equation that describes the transport of HCHO in each model segment or airway of the RT,

$$\frac{\partial C}{\partial t} + \frac{\partial u \cdot C}{\partial z} = D \cdot \frac{\partial^2}{\partial z^2} C - \left(\frac{S \cdot K_o}{V} + \frac{\dot{V}}{V}\right) \cdot C;\ 0 < z < L \quad t > 0. \tag{6}$$

where $\dot{V} = \dot{V}(t) = \frac{dV}{dt}$.

The functional dependence of u on z can be determined by considering C in Equation 6, not as HCHO, but as the concentration of an incompressible gas; i.e., air. In this case,

$$\frac{\partial}{\partial t} C = 0,\ \frac{\partial}{\partial z} C = 0,\ K_o = 0, \text{ and } J = u \cdot C. \text{ Thus,}$$

$$\frac{\partial u}{\partial z} = -\frac{\dot{V}}{V} \text{ with solution, } u = u_0(t) - z \cdot \frac{\dot{V}}{V}. \tag{7}$$

Generally, the airflow rate at (z,t) in a given airway is equal to the time rate of change of the RT volume distal to z; the velocity is

$$u(z,t) = \frac{\frac{\partial}{\partial t} V_{RT}(z,t)}{A(t)}, \tag{8}$$

where $\frac{\partial}{\partial t} V_{RT}(z,t)$ is the time rate change of the LRT volume distal to z.

The dispersion coefficient is defined as

$$D = \left(D_m + \gamma \cdot |\bar{u}| \cdot \frac{L}{3}\right)\left(\frac{V_d}{V}\right); \quad (9)$$

where V_d/V is the ratio of the airway or duct volume to the total volume of the segment; in the URT and TB region, this ratio is 1. D_m is the molecular diffusion coefficient, 0.15 cm^2/s (Kimbell *et al.,* 2001a). $|\bar{u}|$ is defined as the positive value of the average of the air velocities at the left and right boundaries of the airway. The values of γ, listed in Appendix Table 1, depend on the particular RT region and on the direction of the airflow.

APPENDIX TABLE 1
Values of γ in the Formula for Dispersion (Equation 9)

Region or model segment	Inhalation	Exhalation	Source
Numerical segment[a]	0.4[b]	0.4[b]	Present work
Mouth cavity	1.08[c]	0.168[c]	Ben-Jebria *et al.* (1982)
Nasal airway	0.4[d]	0.4[d]	Present work
Distal URT	1.08[c]	0.168[c]	Ben-Jebria *et al.* (1982)
LRT	1.080	0.370	Scherer *et al.* (1975); modified by Miller *et al.* (1985)

[a]The numerical segment (Table 2) is added to the proximal end of the URT to ensure correct boundary conditions (see below).

[b]The value of 0.4 is somewhat arbitrary, but was chosen small enough to minimize dispersion and large enough to ensure stable solutions as well as reasonably short computational times.

[c]Values are 3 times the referenced values because of the factor 1/3 in Equation 9.

[d]The value of 0.4 is somewhat arbitrary. When used in conjunction with the mass transfer coefficient for the nasal airway, the same percent uptake predicted by Kimbell *et al.* (2001b) is obtained, which is required for this segment.

The form of the dispersion coefficient (Equation 9) for each TB segment is based on Scherer *et al.* (1975) as modified by Miller *et al.* (1985). Ben-Jebria *et al.* (1982) presented 2 equivalent representations of the mouth-distal URT dispersion coefficient, 1 in terms of the diameter of the air passage and the other in terms of the length; we chose the latter for consistency with the TB region formulation. For the pulmonary region dispersion coefficient, the concept of flow in a tube ("duct") with stagnant pockets ("alveoli") is used. See Aris (1959) for a discussion of this concept. Based on Verbanck and Paiva (1988), Anjilvel *et al.* (1991), and the parameters used in the present work, Equation 9 for the pulmonary region is a reasonable approximation.

The overall mass transfer coefficient, K_o (see Equations 2 and 6), depends on the gas phase mass transfer coefficient (k_g) and the mass transfer coefficient of the mucus-coated tissue (k_m). For the identical-path dosimetry modeling, K_o can be written as (Overton *et al.,* 1987):

$$K_o = k_m k_g/(k_m + k_g) \quad (10)$$

Except for the nasal airway, the value of k_m, which incorporates the effect of Henry's Law constant, is 4.7 cm/s (Kimbell *et al.,* 2001a) throughout the respiratory tract regardless of the structure or nature of the liquid lining and tissue compartments.

The gas phase mass transfer coefficient (k_g) is dependent on air speed, the segment's hydraulic diameter (d = 4 × volume/[surface area]), molecular diffusion coefficient, and the inhalation or exhalation state:

$$K_g = (a[u \cdot d/D_m]^b + 6)(D_m/d) \quad (11)$$

The first term in the parentheses on the right-hand side is based on Nuckols (1981); the second term, 6, is a modification based on Miller *et al.* (1985) to account for the fact that k_g does not approach 0 when u approaches 0 (i.e., as in the pulmonary region). According to Miller *et al.* (1985) the value of 6 is a reasonable choice as u approaches 0.

Nuckols (1981) did not conduct oronasal breathing experiments. We assume for the nasal airway and mouth cavity that the appropriate k_g is that for nasal and mouth breathing, respectively, regardless of breathing mode. For the distal URT, which receives airflow from both the nose and mouth during oronasal breathing, the "Nuckols" term in Equation 11 is approximated by the geometric mean of the term for oral breathing and the term for nasal breathing:

$$k_g = \left(\sqrt{a_o \cdot a_N} \cdot \left[\frac{u \cdot d}{D_m}\right]^{1/2(b_o + b_N)} + 6\right)\left(\frac{D_m}{d}\right) \quad (12)$$

The subscripts O and N refer to oral breathing and nasal breathing, respectively. The values of a and b for use in Equations 11 and 12 are given in Appendix Table 2.

APPENDIX TABLE 2
Values for the Nuckols (1981) Parameters, a and b, in Equations 11 and 12

	Inhalation		Exhalation	
Region or model segment	a	b	a	b
Nasal airway[a]	n/a	n/a	n/a	n/a
Mouth cavity	0.035	0.804	0.0006[b]	1.269[b]
Distal URT				
Nasal breathing	0.028	0.854	0.0045[c]	1.080[c]
Oral breathing	0.035	0.804	0.0006[b]	1.269[b]
LRT	0.0777	0.726	0.0589	0.752

[a]Values not needed; overall mass transfer coefficient is estimated from the uptake results of Kimbell *et al.* (2001b).

[b]For Reynolds number < 12,000.

[c]For Reynolds number < 7800.

Boundary and initial conditions. At the interface between model segments, concentrations are continuous and mass flow rates of HCHO are conserved. At the most proximal RT boundary (nose and mouth entrance) the concentration is defined as the exposure concentration during inhalation; on exhalation, the gradient of the concentration is defined as 0. At the distal end of the RT path, the flux is 0 at all times.

At the beginning of the first breath of a simulation (t = 0) the air phase concentration is 0 everywhere except at the entrance, where it is equal to the exposure concentration. Simulations are carried out for several breaths until the solution is periodic. Results from periodic solutions are reported.

Numerical formulation. Equation 6 is solved using finite difference techniques. For the interior points of a segment, spatial derivatives are defined in terms of central differences; thus, Equation 6 becomes

$$dC_j/dt = -(w_{j+1} - w_{j-1})/(2h) + D \cdot (C_{j+1} - 2C_j + C_{j-1})/h^2 - E \cdot C_j. \quad (13)$$

In Equation 13, $w = u \times C$ and $j = 2, 3, \ldots, N - 1$. N is the number of equally spaced points along the z axis of the segment, including the boundaries. The distance between the points is h and $E = \left(\frac{S \cdot K_o}{V} + \frac{\dot{V}}{V}\right)$.

At the boundary points of a segment/generation the following equations are used for the left- and right-hand boundaries, respectively:

$$dC_1/dt = 2J_1/h - (w_1 + w_2)/h + 2D(C_2 - C_1)/h^2 - EC_1; \quad (14)$$

$$dC_N/dt = -2J_N/h + (w_{N-1} + w_N)/h - 2D(C_N - C_{N-1})/h^2 - EC_N. \quad (15)$$

(The technique for deriving Equations 14 and 15 is based on and similar to Overton and Graham [1995] for constant u). The subscripts 1 and N refer to the left- and right-hand boundaries of the segment, respectively. Using Equations 14 and 15 at the boundaries of parent and daughter segments and using the boundary conditions for transport across the interface of 2 segments, the flux terms can be eliminated. This results in a differential equation with respect to time for the common concentration at the boundary between segments.

The set of first order differential equations obtained as described above were solved numerically using Euler integration. To decrease the effect of the artificial diffusion that results from using first order time integration, the approach of Owen (1984) was used to redefine the dispersion coefficient for numerical integration by replacing D in Equations 13, 14, and 15 with D_c:

$$D_c = D + 0.5\Delta t(u^2 - 2E \cdot D), \quad (16)$$

where Δt is the time step.

Rationale for Using the Results of Combining 2 Simulations to Approximate Dosimetry for Oronasal Breathing

The rationale behind the method of simulating uptake during oronasal breathing is based on 3 assumptions: (1) Assumption 1 is based on the principle of superposition, which (for our purpose) states that if concentrations C1(x,t) and C2(x,t) are each a solution to Equation 6 with the same set of parameters, then (C1(x,t) + C2(x,t)) is also a solution. We assume that this principal applies to the HCHO molecules breathed in through the nose and to those entering by the mouth. That is, in the RT regions distal to the two proximal URTs, nose and mouth molecules can be treated as being independent of each other, their concentrations can be determined independently, and the total concentration at any position and time can be found by adding the two concentrations. For the two sets of molecules, the instantaneous flux to surfaces is given by $J1 = K_0 \times C1(x,t)$ and $J2 = K_0 \times C2(x,t)$, and the total flux due to both sets of molecules is $J = J1 + J2 = K_0 \times (C1(x,t) + C2(x,t))$. Thus, the total flux at any position and time can be found by adding the two independent fluxes. (2) In the 2-simulation approach, HCHO inhaled through the nose is delivered directly to the proximal URT and the HCHO inhaled through the mouth is delivered directly to the proximal URT and no exchange of HCHO between the nasal airway and the mouth cavity is possible. In actual oronasal breathing, an exchange of HCHO between the mouth cavity and the nasal airway most probably occurs. Thus, we assume that during inhalation, any exchange of HCHO between the nasal airway and the mouth cavity is negligible compared to the transfer from each of the proximal URTs to the distal URT. (3) During exhalation in the 2-simulation approach, all the HCHO mass at the proximal URT and distal URT interface flows into the proximal model segment, which is either the nasal passage or the oral cavity, but not both. In reality, the mass would split along the two different proximal URT paths. Thus, for the 2-simulation approach to be reasonable, proximal URT uptake must be negligible during exhalation. This is supported by the simulation results.

Test of Numerical Procedure and Convergence of Solutions for Identical-Path Dosimetry Model

The computer program that solves the equation describing mass transfer and uptake has been tested by comparing results to known analytical solutions (Overton and Graham, 1995). For these tests, a rigid (nonexpanding/contracting) RT "anatomical" model was used for which there are known solutions to the equation of mass transport. Compared to the known solution, the numerical solution was accurate and showed evidence of converging (absolute difference between analytical and calculated solution decreased) to the analytical solution as the spatial step size and the time step decreased. Convergence is an indication that the numerical formulation of the partial differential equation of mass transfer (Equation 6) is correct.

For testing expansion/contraction, a simulation was performed with no uptake (overall mass transfer coefficients set to 0) for 20 breaths. Results showed that all concentrations within the RT approached the exposure concentration as the number of breaths increased. At the end of 20 breaths, concentrations were essentially constant everywhere in the RT at all times. Although this is a simple and limited test, the results are consistent with expectations.

The present simulations were tested for independence of spatial and time step size and for mass balance. There were 9 different conditions that required simulations, 4 calibration simulations, 4 nasal-path simulations, and 1 oral-path simulation. We chose to perform simulations for spatial step sizes of 1/2, 1/4, and 1/8 of the original size for each of the original 9 simulations. Corresponding to the spatial step size reduction, the time steps were reduced to insure stable solutions by factors of 1/4, 1/16, and 1/64, respectively. Results indicated that further reduction in step sizes would not significantly alter the results.

For a complete breath, the mass balance error is defined as (mass inhaled – mass exhaled – the mass left in the RT) divided by the mass inhaled. In all 36 of the simulations (the 9 different simulation conditions multiplied by 4, the number of different spatial step sizes), the absolute value of the mass balance error was less than 12 parts in 1 million.

REFERENCES

Anjilvel, S., Mercer, R. R., and Crapo, J. D. (1991). Calculation of the effective dispersion coefficient in alveoli and alveolar ducts. *Am. Rev. Respir. Dis.* **144,** A 765.

Aris, R. (1959). The longitudinal diffusion in flow through a tube with stagnant pockets. *Chem. Eng. Sci.* **11,** 194–198.

Batchelor, G. K. (1967). *An Introduction to Fluid Dynamics.* Cambridge University Press, Cambridge, UK.

Ben-Jebria, A., Bedig, G., Mensch, B., and Hatzfeld, C. (1982). Dispersion d'un embole radioactif dans l'oropharynx et le larynx: Recherche de la fonction de transfert. *J. Biophys. et Med. Nucl.* **6**(2), 51–57.

Blair, A., Stewart, P. A., O'Berg, M., Gaffey, W., Walrath, J., Ward, J., Bales, R., Kaplan, S., and Cubit, D. (1986). Mortality among industrial workers exposed to formaldehyde. *J. Natl. Cancer. Inst.* **76,** 1071–1084. [Cited in IARC, 1995]

Blair, A., Stewart, P. A., and Hoover, R. N. (1990). Mortality from lung cancer among workers employed in formaldehyde industries. *Am. J. Ind. Med.* **17,** 683–699. [Cited in IARC, 1995]

Casanova, M., Morgan, K. T., Steinhagen, W. H., Everitt, J. I., Popp, J. A., and Heck, H. d'A. (1991). Covalent binding of inhaled formaldehyde to DNA in the respiratory tract of rhesus monkeys: Pharmacokinetics, rat-to-monkey interspecies scaling, and extrapolation to man. *Fundam. Appl. Toxicol.* **17,** 409–428.

Casanova, M., Morgan, K. T., Gross, E. A., Moss, O. R., and Heck, H. d'A. (1994). DNA-protein cross-links and cell replication at specific sites in the nose of F344 rats exposed subchronically to formaldehyde. *Fundam. Appl. Toxicol.* **23,** 525–536.

Casanova, M., Heck, H. d'A., Everitt, J. I., Harrington, W. W., Jr., and Popp, J. A. (1988). Formaldehyde concentrations in the blood of rhesus monkeys after inhalation exposure. *Food Chem. Toxicol*. **26,** 715–716.

Collins, J. J., Acquavella, J. F., and Esmen, N. A. (1997). An updated meta-analysis of formaldehyde exposure and upper respiratory cancers. *J. Occup. Environ. Med*. **39,** 639–651.

Fredberg, J. J., Whol, M. E. B., Glass, G. M., and Dorkin, H. L. (1980). Airway area by acoustic reflections measured at the mouth. *J. Appl. Physiol.* **48,** 749–758.

Gardner, M. J., Pannett, B., Winter, P. D., and Cruddas, A. M. (1993). A cohort study of workers exposed to formaldehyde in the British chemical industry: An update. *Br. J. Ind. Med*. **50,** 827–834. [Cited in IARC, 1995]

Godo, M. N., Morgan, K. T., Richardson, R. B., and Kimbell, J. S. (1995). Reconstruction of complex passageways for simulations of transport phenomena: Development of a graphical user interface for biological applications. *Comp. Meth. Prog. Biomed.* **47,** 97–112.

Hart, M. C., Orzalesi, M. M., and Cook, C. D. (1963). Relation between anatomic respiratory dead space and body size and lung volume. *J. Appl. Physiol*. **18**(3), 519–522.

Health and Welfare Canada. (1987). *Exposure Guidelines for Residential Indoor Air Quality. A Report of the Federal-Provincial Advisory Committee on Environmental and Occupational Health.* Environmental Health Directorate, Health Protection Branch, Ottawa.

Hobler, T. (1966). *Mass Transfer and Absorbers*. Pergamon Press, New York.

IARC (1982). *IARC Monographs on the Evaluation of the Carcinogenic Risk of Chemicals to Humans. Some Industrial Chemicals and Dyestuffs*, Vol. 29, pp. 345–389. International Agency for Research on Cancer, Lyon, France.

IARC (1987). *Asbestos IARC Monographs on the Evaluation of Carcinogenic Risks to Humans, Suppl. 7, Overall Evaluations of Carcinogenicity: An Updating of IARC Monographs*, Vol. 1–42, pp. 106–116. International Agency for Research on Cancer, Lyon, France.

IARC (1995). Formaldehyde. In *Formaldehyde IARC Monographs on the Evaluation of Carcinogenic Risks to Humans*, Vol. 62, pp. 217–362. International Agency for Research on Cancer, Lyon, France.

ICRP66 (1994). Human Respiratory Tract Model for Radiological Protection. In *Annals of the ICRP*, Vol. 24(1–3). Publication 66. International Commission on Radiological Protection.

Kepler, G. M., Richardson, R. B., Morgan, K. T., and Kimbell, J. S. (1998). Computer simulation of inspiratory nasal airflow and inhaled gas uptake in a rhesus monkey. *Toxicol. Appl. Pharmacol.* **150,** 1–11.

Kerns, W. D., Pavkov, K. L., Donofrio, D. J., Gralla, E. J., and Swenberg, J. A. (1983). Carcinogenicity of formaldehyde in rats and mice after long-term inhalation exposure. *Cancer Res.* **43,** 4382–4392.

Kimbell, J. S., Godo, M. N., Gross, E. A., Joyner, D. R., Richardson, R. B., and Morgan, K. T. (1997a). Computer simulation of inspiratory airflow in all regions of the F344 rat nasal passages. *Toxicol. Appl. Pharmacol.* **145,** 388–398.

Kimbell, J. S., Gross, E. A., Joyner, D. R., Godo, M. N. and Morgan, K. T. (1993). Application of computational fluid dynamics to regional dosimetry of inhaled chemicals in the upper respiratory tract of the rat. *Toxicol. Appl. Pharmacol*. **121,** 253–263.

Kimbell, J. S., Gross, E. A., Richardson, R. B., Conolly, R. B., and Morgan, K. T. (1997b). Correlation of regional formaldehyde flux predictions with the distribution of formaldehyde-induced squamous metaplasia in F344 rat nasal passages. *Mutat. Res.* **380**(1–2), 143–154.

Kimbell, J. S., Overton, J. H., Subramaniam, R. P., Schlosser, P. M., Morgan, K. T., Conolly, R. B., and Miller, F. J. (2001a). Dosimetry modeling of inhaled formaldehyde: Binning nasal flux predictions for quantitative risk assessment. *Toxicol. Sci.* **64,** 111–121.

Kimbell, J. S, Subramaniam, R. P., Gross, E. A., Schlosser, P. M., and Morgan, K. T. (2001b). Dosimetry modeling of inhaled formaldehyde: Comparisons of local flux predictions in the rat, monkey, and human nasal passages. *Toxicol. Sci.* **64,** 100–110.

Lodén, M. (1986). The *in vitro* permeability of human skin to benzene, ethylene glycol, formaldehyde, and n-hexane. *Acta Pharmacol. Toxicol.* **58,** 382–389.

Miller, F. J., Overton, J. H., Jaskot, R. H., and Menzel, D. B. (1985). A model of the regional uptake of gaseous pollutants in the lung. I. The sensitivity of the uptake of ozone in the human lung to lower respiratory tract secretions and exercise. *Toxicol. Appl. Pharmacol.* **79,** 11–27.

Monticello, T. M., Morgan, K. T., Everitt, J. I., and Popp, J. A. (1989). Effects of formaldehyde on the respiratory tracts of rhesus monkeys: Pathology and cell proliferation. *Am. J. Pathol*. **134,** 515–527.

Monticello, T. M., Miller, F. J., and Morgan, K. T. (1991). Regional increases in rat nasal epithelial proliferation following acute and subchronic inhalation of formaldehyde. *Toxicol. Appl. Pharmacol*. **111,** 409–421.

Niinimaa, V., Cole, P., Mintz, S., Shephard, R. J. (1981). Oronasal distribution of respiratory airflow. *Respir. Physiol*. **43,** 69–75.

Niinimaa, V., Cole, P., Mintz, S., Shephard, R. J. (1980). The switching point from nasal to oronasal breathing. *Respir. Physiol.* **42,** 61–71.

Nuckols, M.L. (1981). Heat and water vapor transfer in the human respiratory system at hyperbaric conditions. Ph.D. Dissertation, Duke University, Durham, NC.

Overton, J. H., Barnett, A. E., and Graham, R. C. (1989). Significances of the variability of tracheobronchial airway paths and their air flow rates to dosimetry model predictions of the absorption of gases. In *Extrapolation of Dosimetric Relationships for Inhaled Particles and Gases* (Crapo, J. D., Smolko, E. D., Miller, F. J., Graham, J. A., and Hayes, A.W., Eds.), pp. 273–291. Academic Press, San Diego, CA.

Overton, J. H., and Graham, R. C. (1994). Modeling the uptake of gases by the dog nasal-pharyngeal region: Effects of morphometric and physiological factors. *Inhal. Toxicol.* **6**(Suppl.), 113–124.

Overton, J. H. and Graham, R. C. (1995). Simulation of the uptake of a reactive gas in a rat respiratory tract model with an asymmetric tracheobronchial region patterned on complete conducting airway cast data. *Comput. Biomed. Res.* **28,** 171–190.

Overton, J. H., Graham, R. C., Ménache, M. G., Mercer, R. R., and Miller, F. J. (1996). Influence of tracheobronchial region expansion and volume on reactive gas uptake and interspecies dose extrapolations. *Inhal. Toxicol.* **8,** 723–745.

Overton, J. H., Graham, R. C., and Miller, F. J. (1987). A model of the regional uptake of gaseous pollutants in the lung. II. The sensitivity of ozone uptake in laboratory animal lungs to anatomical and ventilatory parameters. *Toxicol. Appl. Pharmacol*. **88,** 418–432.

Owen, A. (1984). Artificial diffusion in the numerical modeling of advective transport of salinity. *Appl. Math. Modeling* **8,** 116–120.

Paiva, M. (1973). Gas transport in the human lung. *J. Appl. Physiol.* **35,** 401–410.

Patterson, D. L., Gross, E. A., Bogdanffy, M. S., and Morgan, K. T. (1986). Retention of formaldehyde gas by the nasal passages of F-344 rats. *Toxicologist* **6,** 55.

Phalen, R. F., and Oldham, M. J. (1983). Tracheobronchial airway structure as revealed by casting techniques. *Am. Rev. Respir. Dis*. **128,** S1–S4.

Scherer, P. W., Gobran, S., Aukburg, S. J., Baumgardner, J. E., Bartkowski, R., and Neufeld, G. R. (1988). Numerical and experimental study of steady-state CO_2 and inert gas washout. *J. Appl. Physiol.* **64**, 1022–1029.

Scherer, P. W., Shendalman, L. H., and Green, N. M. (1972). Simultaneous diffusion and convection in single breath lung washout. *Bull. Math. Biophys.* **35,** 393–412.

Scherer, P. W., Shendalman, L. H., Greene, N. M., and Bouhuys, A. (1975).

Measurement of axial diffusivities in a model of the bronchial airways. *J. Appl. Physiol*. **38**, 719–723.

Stayner, L. T., Elliott, L., Blade, L., Keenlyside, R., and Halperin, W. (1988). A retrospective cohort mortality study of workers exposed to formaldehyde in the garment industry. *Am. J. Ind. Med.* **13,** 667–681.

Subramaniam, R. P., Richardson, R. B., Morgan, K. T., Guilmette, R. A., and Kimbell, J. S. (1998). Computational fluid dynamics simulations of inspiratory airflow in the human nose and nasopharynx. *Inhal. Toxicol.* **10,** 92–120.

Swenberg, J. A., Kerns, W. D., Mitchell, R. I., Gralla, E. J., and Pavkov, P. L. (1980). Induction of squamous cell carcinomas of the rat nasal cavity by inhalation exposure to formaldehyde vapor. *Cancer Res.* **40,** 3398–3402.

U.S. Consumer Product Safety Commission (U. S. CPSC). (1982). Part IV: Consumer Product Safety Commission ban of urea formaldehyde foam insulation, withdrawal of proposed labeling rule, and denial of petition to issue a standard. *47 Fed. Regist.* 14366–14419.

U.S. EPA (1986). *Guidelines for Carcinogen Risk Assessment*. U.S. Environmental Protection Agency. *51 Fed. Regist.* 33992–34005.

U.S. EPA (1987). *Assessment of Health Risks to Garment Workers and Certain Home Residents from Exposure to Formaldehyde*. Office of Pesticides and Toxic Substances, U.S. Environmental Protection Agency, Washington, D.C.

U.S. EPA (1988). *Recommendations for and Documentation of Biological Values for Use in Risk Assessment*, EPA–600/6–87–008. Environmental Criteria and Assessment Office, Office of Health and Environmental Assessment, U.S. Environmental Protection Agency, Cincinnati, OH.

U.S. EPA (1991). *Formaldehyde Risk Assessment Update – Final Draft*. Office of Toxic Substances, U.S. Environmental Protection Agency, Washington, D.C.

U.S. EPA (1992). An SAB Report: Formaldehyde Risk Assessment Update. Review of the Office of Toxic Substance's Draft Formaldehyde Risk Assessment Update by the Environmental Health Committee. Science Advisory Board. U.S. Environmental Protection Agency. EPA–SAB–EHC–92–021.

U.S. EPA (1994). *Methods for Derivation of Inhalation Reference Concentrations and Application of Inhalation Dosimetry*, EPA/600/8–90–066F. Office of Health and Environmental Assessment, U.S. Environmental Protection Agency, Washington, D.C.

U.S. EPA (1996). *Proposed Guidelines for Carcinogen Risk Assessment*, EPA/600/P–92/003C. Office of Research and Development, U.S. Environmental Protection Agency, Washington, D.C.

Verbanck, S., and Paiva, M. (1988). Effective axial diffusion in an expansile alveolar duct model. *Respir. Physiol.* **73,** 273–278.

Weibel, E. R. (1963). *Morphometry of the Human Lung*. Academic Press, New York.